Modeling Inclement Weather Impacts on Traffic Stream Behavior

Hesham Rakha, PhD., P.Eng.[1,*], Mazen Arafeh[2], Sangjun Park[3]
[1]Charles E. Via, Jr. Department of Civil and Environmental Engineering
Virginia Tech Transportation Institute, 3500 Transportation Research Plaza,
Blacksburg, VA 24061, USA. Phone: (540) 231-1505, FAX: (540) 231-1555
hrakha@vt.edu
[2,3]Virginia Tech Transportation Institute, 3500 Transportation Research Plaza,
Blacksburg, VA 24061, USA. Phone: (540) 231-1509, FAX: (540) 231-1555
[2]amazen@vt.edu [3]sangjun@vt.edu

ABSTRACT

The research identifies the steady-state car-following model parameters within state-of-the-practice traffic simulation software that require calibration to reflect inclement weather and roadway conditions. The research then develops procedures for calibrating non-steady state car-following models to capture inclement weather impacts and applies the procedures to the INTEGRATION software on a sample network. The results demonstrate that the introduction of rain precipitation results in a 5% reduction in light-duty vehicle speeds and a 3% reduction in heavy-duty vehicle speeds. An increase in the rain intensity further reduces light-duty vehicle and heavy-duty truck speeds resulting in a maximum reduction of 9.5% and 5.5% at the maximum rain intensity of 1.5 cm/h, respectively. The results also demonstrate that the impact of rain on traffic stream speed increases with the level of congestion and is more significant than speed differences attributed to various traffic operational improvements and thus should be accounted for in the analysis of alternatives. In the case of snow precipitation, the speed reductions are much more significant (in the range of 55%). Furthermore, the speed reductions are minimally impacted by the snow precipitation intensity. The study further demonstrates that precipitation intensity has no impact on the relative merit of various scenarios (i.e. the ranking of the scenario results are consistent across the various rain intensity levels). This finding is important given that it demonstrates that a recommendation on the optimal scenario is not impacted by the weather conditions that are considered in the analysis.

INTRODUCTION

The Highway Capacity Manual [1] (HCM) asserts that adverse weather can significantly reduce operating speeds and identifies when and how these effects occur. The manual references several studies in its discussion of weather effects.

The rapid development of personal computers over the last few decades has provided the necessary computing power for advanced traffic micro-simulators. Today, microscopic traffic simulation software are widely accepted and applied in all branches of transportation engineering as an efficient and cost effective analysis tool. One of the main reasons for this popularity is the ability of microscopic traffic simulation software to reflect the dynamic nature of the transportation system in a stochastic fashion. The HCM recommends the use of microscopic simulation for conditions that go beyond the typical HCM applications.

The core of microscopic traffic simulation software is a car-following model that characterizes the longitudinal motion of vehicles. The process of car-following consists of two levels, namely modeling steady-state and non-steady-state behavior [2]. Ozaki defined steady state as conditions in which the vehicle acceleration and deceleration rate is within a range of ±0.05g [3]. Another definition of steady-state or stationary conditions is provided by Rakha [4] as the conditions when traffic states remain practically constant over a short time and distance. Steady-state car-following is extremely critical to traffic stream modeling given that it influences the overall behavior of the traffic stream. Specifically, it determines the desirable speed of vehicles at different levels of congestion, the roadway capacity, and the spatial extent of queues. Alternatively, non-steady-state conditions govern the behavior of vehicles while moving from one steady state to another through the use of acceleration and deceleration models. The acceleration model is typically a function of the vehicle dynamics while the deceleration model ensures that vehicles maintain a safe relative distance to the preceding vehicle thus ensuring that the traffic stream is asymptotically stable. Both acceleration and deceleration models can affect steady-state conditions by reducing queue discharge saturation flow rates.

Traffic stream models describe the motion of a traffic stream by approximating for the flow of a continuous compressible fluid. The traffic stream models relate three traffic stream measures, namely: flow rate (q), density (k), and space-mean-speed (u). Gazis et al. [5] were the first to derive the bridge between microscopic car-following and macroscopic traffic stream models. Specifically, the flow rate can be expressed as the inverse of the average vehicle time headway. Similarly, the traffic stream density can be approximated for the inverse of the average vehicle spacing for all vehicles within a section of roadway. Therefore every car-following model can be represented by its resulting steady-state traffic stream model. Different graphs relating each pair of the above parameters can be used to show the steady-state properties of a particular model; including the speed-spacing (u-s) and speed-flow-density (u-q-k) relationships. The latter curve is of more interest, since it is more sensitive to the calibration process and the shape and nose position of the curve determines the behavior of the resulting traffic stream.

A reliable use of micro-simulation software requires a rigorous calibration effort.

Because traffic simulation software are commonly used to estimate macroscopic traffic stream measures, such as average travel time, roadway capacity, and average speed, the state-of-the-practice is to systematically alter the model input parameters to achieve a reasonable match between desired macroscopic model output and field data [6]. Since the macroscopic flow characteristics are mostly related to steady-state conditions, this requires the user to calibrate the parameters of the steady-state relationship and therefore the knowledge of the steady-state behavior of the car-following model is necessary in this process.

The goals of this paper are three-fold. First, the paper identifies the steady-state car-following model parameters that require calibration to reflect inclement weather and roadway conditions. Second, the paper develops a procedure for calibrating non-steady state car-following models to capture inclement weather impacts. Finally, the paper applies these procedures to a sample network to demonstrate the potential network-wide impacts of inclement weather.

INCLEMENT WEATHER IMPACT OF TRAFFIC STREAM BEHAVIOR

An earlier publication [7] developed weather adjustment factors (WAFs) for three key traffic stream parameters (u_f, u_c, and q_c). These WAFs vary as a function of the precipitation type (rain and snow), intensity level, and visibility level as

$$WAF = a_1 + a_2\ i + a_3\ i^2 + a_4\ v + a_5\ v^2 + a_6 iv \tag{1}$$

Here i is the precipitation intensity (cm/h), v is the visibility level (km), (iv) is the interaction term between precipitation and visibility, and a_1 through a_6 are calibrated model parameters.

A stepwise regression analysis was performed using the Minitab software [8]. Stepwise regression removes and adds variables to the regression model for the purpose of identifying a useful subset of predictors. The coefficients and statistics for the best model for each dataset were generated by running the stepwise regression tool. Recognizing that automatic procedures cannot take into account the specific knowledge the analyst may have about the data, a validity check was made. This validity check ensured that the data did not produce unrealistic trends (e.g. the weather adjustment factors increased as the precipitation intensity increased). While such a model may be the best from a statistical standpoint, that may not be the case from a practical standpoint. In these rare cases, the model was constrained to ensure that it produced realistic trends. The various models that were developed for the three parameters u_f, u_c, and q_c are summarized in Table 1.

MODELING VEHICLE DECELERATION AND ACCELERATION BEHAVIOR

This section briefly describes the physics of vehicle deceleration and acceleration modeling using a vehicle dynamics approach. In addition, a procedure for accounting for the impact of inclement weather and roadway conditions on vehicle deceleration and acceleration behavior is developed and discussed.

Table 1: Regression Analysis Summary Results

	Precipit.	City	n	a_1	a_2	a_3	a_4	a_5	a_6	P-val.	R^2_{Adj}	Normality Test		Levene's Variance Test P-value
												A^2	P-value	
u_f	Rain	Baltimore	32	0.963 (0.000)	-0.033 (0.001)	---	---	---	---	0.001	0.304	0.485	0.211	0.684
		Twin Cities	45	0.980 (0.000)	-0.0274 (0.000)	---	---	---	---	0.000	0.540	0.553	0.146	0.424
		Seattle	43	0.973 (0.000)	-0.0650 (0.000)	0.0240 (0.004)	---	0.0010 (0.044)	---	0.000	0.607	0.336	0.493	0.067
	Snow	Baltimore	8	0.955	---	---	---	---	---	---	---	---	---	---
		Twin Cities	32	0.842 (0.000)	-0.131 (0.002)	---	---	0.0055 (0.000)	---	0.000	0.866	0.456	0.251	0.704
		Aggregated	40	0.838 (0.000)	-0.0908 (0.025)	---	---	0.00597 (0.000)	---	0.000	0.824	0.340	0.482	0.624
u_c	Rain	Baltimore	35	0.920 (0.000)	-0.0560 (0.003)	---	---	---	---	0.003	0.236	0.581	0.120	0.989
		Twin Cities	53	0.928	---	---	---	---	---	---	---	---	---	---
		Seattle	50	0.906	---	---	---	---	---	---	---	---	---	---
	Snow	Baltimore	8	0.955	---	---	---	---	---	---	---	---	---	---
		Twin Cities	41	0.852 (0.000)	---	---	0.0226 (0.000)	---	---	0.000	0.497	---	0.828	0.864
q_c	Rain	Baltimore	35	0.892	---	---	---	---	---	---	---	---	---	---
		Twin Cities	43	0.889	---	---	---	---	---	---	---	---	---	---
		Seattle	49	0.896	---	---	---	---	---	---	---	---	---	---
	Snow	Baltimore	6	0.877 (0.000)	---	---	---	---	---	---	---	---	---	---
		Twin Cities	38	0.794 (0.000)	---	---	---	0.00508 (0.000)	---	0.000	0.480	0.318	0.524	0.859

Vehicle Deceleration Behavior

The literature [9] indicates that the maximum braking force acting on each axle can be computed as the coefficient of roadway adhesion multiplied by the vehicle weight normal to the roadway surface. Because true optimal brake force proportioning is seldom achieved in standard non-antilock braking systems, a braking efficiency term is also used in computing the maximum braking force as

$$d_{max} = \eta_b \mu g \, . \tag{2}$$

Here η_b is the braking efficiency, μ is the coefficient of roadway adhesion also known as the coefficient of friction, and g is the gravitational acceleration (9.8066 m/s^2). In the case of antilock braking systems the braking efficiency approaches 100%. Noteworthy is the fact that Equation (2) demonstrates that the maximum vehicle deceleration varies as a function of the roadway conditions as reflected by the coefficient of road friction.

Typical values for the maximum value for the coefficient of roadway adhesion for good roadway surfaces range from 1.00 (maximum) to 0.80 (sliding), as summarized in Table 2. A wet pavement results in a decrease in the coefficient of road adhesion by at least 10%. Snow reduces the coefficient of roadway adhesion by more than 50%. Typical values for the coefficient of friction are provided in Table 3.

Table 2: Maximum Values of Coefficients of Road Adhesion (Source: [9])

Pavement	Coefficient of Road Adhesion	
	Maximum	Slide
Good, dry	1.00	0.80
Good, wet	0.90	0.60
Poor, dry	0.80	0.55
Poor, wet	0.60	0.30
Packed snow or ice	0.25	0.10

In quantifying the impact of inclement weather on driver deceleration behavior, data from an infrastructure-based radar and video data collection system were utilized. The system measured a variety of state and kinematic information (such as brake status, acceleration level, and velocity) for vehicles at five stop-controlled and three four-way signalized intersections for two months at each location. Data were collected and analyzed with the goal of understanding how drivers approach intersections under various approach speeds and environmental conditions.

The Data Acquisition System (DAS) employed a suite of hardware and software to record information on vehicles approaching the test sites. The DAS was composed of:

1. A radar that was mounted on each of the four signal mast arms to provide parametric vehicle data. The high-performance radar system had an advertised position accuracy of 0.5 m with a range of 0.5 m to more than 200 m. Speed accuracy is

advertised at better than 1 percent. A single radar was mounted on each of the four mast arms below a video camera and aimed directly at the approaching traffic.

2. A video camera was installed on each of the four traffic signal mast arms to provide an image of the entire intersection environment.
3. A weather station was installed at each intersection to gather weather data at one-minute intervals. The collected weather data included long-term rain fall, daily rain fall, wind direction, wind speed, average wind speed, temperature, barometric pressure, and humidity level.

Table 3: Rolling and Friction Coefficient Values based on Roadway Surface Condition (Source: [10])

Pavement type	Pavement Condition	C_r	Coefficient of Friction
Concrete	Excellent	1.00	0.80
	Good	1.50	0.70
	Poor	2.00	0.60
Asphalt	Good	1.25	0.60
	Fair	1.75	0.50
	Poor	2.25	0.40
Macadam	Good	1.50	0.55
	Fair	2.25	0.45
	Poor	3.75	0.35
Cobbles	Ordinary	5.50	0.50
	Poor	8.50	0.40
Snow	2”	2.50	0.20
	4”	3.75	0.15
Dirt	Smooth	2.50	0.30
	Sandy	3.75	0.20
Mud		3.75 – 15.0	0.15
Sand	Level soft	6.0 – 15.0	0.15
	Dune	16.0 – 30.0	0.10

Data were extracted for one of the signalized intersections using two months worth of data. The data included vehicle trajectories that appeared at least 50 m upstream of the approach stop line and decelerated to a final speed of less than 5 m/s. The number of deceleration maneuvers that met the criteria decreased as the rain intensity increased, as illustrated in Figure 1. The rain intensities ranged from 0.3 to 7.0 cm/h. The maximum deceleration level (minimum acceleration level) for each deceleration maneuver was extracted from the data.

The minimum acceleration levels were further reduced by selecting the five minimum acceleration observations for each precipitation level. A regression model was fit to the data, as illustrated in Table 4. The response variable considered was the acceleration level and two independent variables were considered, namely: the vehicle initial speed and the rain intensity. The coefficient of determination of the model was 74% and both

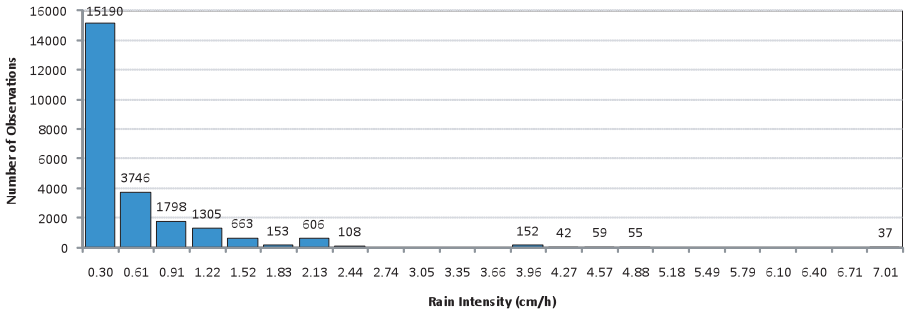

Figure 1: Number of Vehicle Trajectories as a Function of Rain Intensity

Table 4: Impact of Rain Intensity on Driver Deceleration Behavior

Regression Statistics	
Multiple R	0.863
R^2	0.745
Adj. R^2	0.737
Standard Error	0.047
Observations	65

ANOVA

	df	SS	MS	F	Sig. F
Regression	2	0.406	0.203	90.558	0.000
Residual	62	0.139	0.002		
Total	64	0.545			

	Coefficients	Std. Error	t Stat	P-value	Lower 95%	Upper 95%
Intercept	-0.4245	0.0272	-15.6240	0.0000	-0.4788	-0.3702
Rain Intensity (cm/h)	0.0393	0.0030	12.9575	0.0000	0.0332	0.0453
Speed (km/h)	-0.0058	0.0017	-3.3477	0.0014	-0.0093	-0.0023

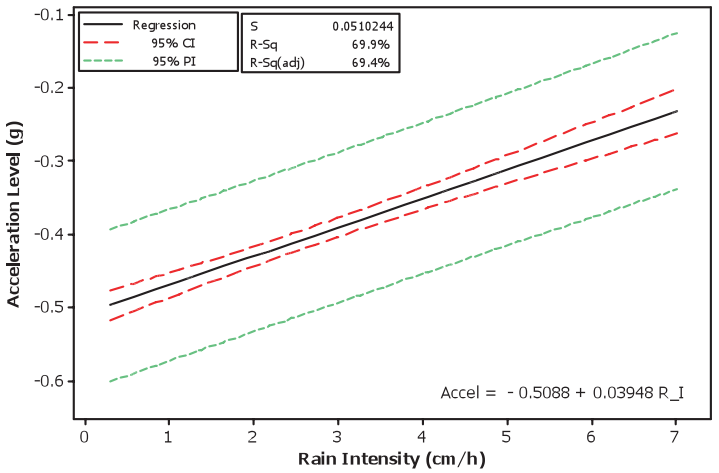

independent variables were found to be significant ($p<0.05$), as summarized in Table 4. A test of normality on the response variable demonstrated that there was insufficient evidence to reject the normality hypothesis (Anderson-Darling value of 0.465 and a p-value of 24.6%). It should be noted that the slope of the line in the single-variable model (0.03945) is practically identical to that in the two-parameter model (0.0393), and thus the effect of rain intensity is similar regardless of the model.

Using the proposed model the deceleration behavior within microscopic traffic simulation software can be modified to account for the effect of precipitation on driver/vehicle behavior. Specifically, the maximum vehicle deceleration can be computed as

$$d_{max} = \left(0.5088 - 0.03948i\right)g = \eta_b \mu g\left(1.0 - 0.07759i\right). \tag{3}$$

Here the maximum deceleration rate is adjusted using a rain adjustment factor that accounts for the impact of rain intensity on the deceleration behavior. Once the maximum deceleration rate is computed, the traffic simulation software can be calibrated, as will be discussed later in the paper.

Vehicle Acceleration

Vehicle acceleration is governed by vehicle dynamics. Vehicle dynamics models compute the maximum vehicle acceleration levels from the resultant force acting on a vehicle, as

$$a = f_p \frac{F - R}{m} \tag{4}$$

where a is the vehicle acceleration (m/s^2), F is the vehicle tractive force (N), R is the total resistance force (N), m is the vehicle mass (kg), and f_p is the proportion of the maximum acceleration that the driver is willing to employ (field studies have shown that it is typically 0.62). Given that acceleration is the second derivative of distance with respect to time, Equation (4) resolves to a second-order Ordinary Differential Equation (ODE) of the form

$$\frac{d^2x}{dt^2} = f\left(\frac{dx}{dt}, x\right). \tag{5}$$

The vehicle tractive effort is computed as

$$F_T = 3600\ \beta\,\eta\,\frac{P}{u}. \tag{6}$$

Here F_T is the engine tractive force (N), β is a gear reduction factor that will be described later (unitless), μ is the driveline efficiency (unitless), P is the vehicle power (kW), and u is the vehicle speed (km/h).

Given that the tractive effort tends to infinity as the vehicle speed tends to zero, the tractive force cannot exceed the maximum force that can be sustained between the vehicle's tractive axle tires and the roadway surface, which is computed as

$$F_{max} = m_{ta}\, g\mu\,. \tag{7}$$

Here m_{ta} is the mass of the vehicle on the tractive axle (kg), g is the gravitational acceleration (9.8066 m/s^2), and μ is the coefficient of road adhesion or the coefficient of friction (unitless).

Typical axle mass distributions for different truck types were presented in an earlier publication and thus are not discussed further [10]. The tractive force is then computed as the minimum of the two forces as

$$F = \min(F_T, F_{max})\,. \tag{8}$$

Rakha and Lucic [11] introduced the β factor into Equation (6), in order to account for the gear shift impacts at low traveling speeds when trucks are accelerating. While the variable power factor does not incorporate gear shifts explicitly, it does account for the major behavioral characteristics that result from gear shifts, namely the reductions of power. Specifically, the factor is a linear function of vehicle speed with an intercept of $1/u_0$ and a maximum value of 1.0 at u_0 (optimum speed or the speed at which the vehicle attains its full power) as

$$\beta = \frac{1}{u_0}\left[1 + \min\left(u, u_0\right)\left(1 - \frac{1}{u_0}\right)\right]. \tag{9}$$

The intercept guarantees that the vehicle has enough power to accelerate from a complete stop. The calibration of the variable power factor was conducted by experimenting with different truck and weight combinations to estimate the speed at which the vehicle power reaches its maximum (termed the optimum speed). The optimum speed was found to vary as a function of the weight-to-power ratio (for weight-to-power ratios (w) ranging from 30 to 170 kg/kW) as

$$u_0 = 1164 w^{-0.75}\,. \tag{10}$$

Here w is the weight-to-power ration in kg/kW. Rakha and Snare [12] demonstrated that the gear shift parameter β is not required for the modeling of light-duty vehicle acceleration behavior (weight-to-power is less than 30 kg/kW).

Three resistance forces are considered in the model, namely the aerodynamic, rolling, and grade resistance forces [9, 10]. The first resistance force is the aerodynamic resistance that varies as a function of the square of the air speed. Although a precise description of the various forces would involve the use of vectors, for most transportation applications scalar equations suffice if the forces are considered to only apply in the roadway longitudinal direction. For the motion of a vehicle in still air, the air speed equals the vehicles speed as

$$R_a = \frac{\rho}{2 \times 3.6^2} C_d C_h A u^2 = c_1 C_d C_h A u^2\,, \tag{11}$$

where ρ is the density of air at sea level and a temperature of 15ºC (59ºF) (equal to 1.2256 kg/m^3), C_d is the drag coefficient (unitless), C_h is a correction factor for altitude (unitless), and A is the vehicle frontal area (m^2). Given that the air density varies as a function of altitude, the C_h factor can be computed as

$$C_h = 1 - 8.5 \times 10^{-5} H \,. \tag{12}$$

Typical values of vehicle frontal areas for different vehicle types and typical drag coefficients are provided in the literature [10].

The second resistance force is the rolling resistance, which is a linear function of the vehicle speed and mass, as

$$R_r = C_r \left(c_2 u + c_3\right) \frac{mg}{1000} \,. \tag{13}$$

Typical values for the rolling coefficients (C_r, c_1, and c_2), as a function of the road surface type, condition, and vehicle tires, are provided in the literature [10]. Generally, radial tires provide a resistance that is 25 percent less than that for bias ply tires. Typical values of Cr as a function of the roadway surface are summarized in Table 3.

The third and final resistance force is the grade resistance, which accounts for the proportion of the vehicle weight that resists the movement as a function of the roadway grade (i) as

$$R_g = mgi \ . \tag{14}$$

Having computed the various resistance forces, the total resistance force is computed as

$$R = R_a + R_r + R_g \,. \tag{15}$$

Using vehicle dynamics models it is possible to compute the maximum possible acceleration a vehicle is willing to exert based on Equation (4). The vehicle dynamics model will be utilized to calibrate the first term of Equation (17), as will be discussed later in the paper.

CAR-FOLLOWING MODEL CALIBRATION

Over the last few decades, several car-following models have been developed and incorporated within micro-simulation software packages. A description of the characteristics of six of the state-of-practice and state-of-art car-following models, including the Pitt model (CORSIM) [13], Gipps' model (AIMSUN2) [14-16], Wiedemann74 and 99 models (VISSIM), Fritzsche's model (PARAMICS) [17], and the Van Aerde model (INTEGRATION) [18, 19] were discussed by Rakha and Gao [20]. These car-following models are briefly described in the following sub-sections.

The Pitt car-following model that is used in the CORSIM software can be cast as

$$s_n(t) = s_j + c_3 \frac{u_n(t+\Delta t)}{3.6} + bc_3 \frac{\Delta u_n(t+\Delta t)^2}{3.6^2}, \tag{16}$$

where $s_n(t)$ is the vehicle spacing between the front bumper of the lead vehicle and front bumper of following vehicle at time t (m), s_j is the vehicle spacing when vehicles are completely stopped in a queue (m), c_3 is the driver sensitivity factor (s), b is a calibration constant that equals 0.1 if the speed of the following vehicle exceeds the speed of the lead vehicle, otherwise it is set to zero (h/km), Δu is the difference in speed between lead and following vehicle (km/h) at instant $t+\Delta t$, and u_n is the speed of the following vehicle at instant t (km/h).

The Gipps' model assumes that vehicles travel as close to their desired speed as possible within their constraints of vehicle dynamics as

$$u_n(t+T) = \min \left(\begin{array}{l} u_n(t) + 3.6\left[2.5a_n T(1 - \frac{u_n(t)}{U_n}) \sqrt{0.025 + \frac{u_n(t)}{U_n}} \right], \\ 3.6\left[-bT + \sqrt{b^2T^2 + b\{2\left[s_n(t) - L_{n-1} \right] - u_n(t)T + \frac{u_{n-1}(t)^2}{b'}\}} \right] \end{array} \right). \tag{17}$$

Here $u_n(t)$ is the speed of vehicle n at time t (km/h); a_n is the maximum desired acceleration rate of vehicle n (m/s^2); T it the driver's reaction time (s); U_n is the desired speed of vehicle n or the vehicle-specific free-flow speed (km/h); b and b' are deceleration parameters of vehicle n (m/s^2); b is the actual most severe deceleration rate the vehicle is willing to employ in order to avoid a collision; and b' is the estimated most severe deceleration rate the leader vehicle is willing to employ. It is an estimated value because it is impossible for the follower to evaluate the real intention of his/her leader; L_{n-1} is the effective length of vehicle n-1 (the actual length plus a safety margin); $s_n(t)$ is the spacing between vehicle n and n-1 at time t (m); and $u_{n-1}(t)$ is the speed of the preceding vehicle (km/h).

In the case of the Wiedemann74 model, the desired vehicle spacing is an interval ($ABX \leq s \leq SDX$) instead of a single value as was the case with previously mentioned models. Given that $\Delta u_n|0$ under steady-state conditions, only the boundaries of desired vehicle spacing interval (ABX & SDX) determine the steady-state characteristics of the VISSIM car-following model. The expected value of ABX and SDX parameters can be calculated as

$$E(AX) = s_j + AXadd + AXmult \cdot E(RND1_n) = s_j + 0.5 \approx s_j, \tag{18}$$

$$E(ABX) = E(AX) + E(BX)\sqrt{u} = s_j + E(BX)\sqrt{u}, \quad u \leq u_{desired}, \text{ and} \tag{19}$$

$$E\left(SDX\right) = s_j + E\left(BX\right) \cdot E\left(EX\right)\sqrt{u}, \qquad u \le u_{desired}\,. \tag{20}$$

Where the BX and EX random variables are computed as

$$BX = BXadd + BXmult \cdot RND1_n\text{, and} \tag{21}$$

$$EX = EXadd + BXmult \cdot \left(NRND - RND2_n\right). \tag{22}$$

Here $RND1_n$ and $RND2_n$ are user specified vehicle-specific (where n is the vehicle index) normally distributed random variables with a default mean value of 0.5 and a standard deviation of 0.15. $NRND$ is also a normally distributed random variable with a default mean value of 0.5 and standard deviation of 0.15. The expectation of SDX given as $\mathrm{E}(SDX)$ ranges between 1.5 to 2.5 times the expected value of ABX $(\mathrm{E}(ABX))$, where BX_{add}, BX_{mult}, EX_{add}, and EX_{mult} are user-defined calibration parameters.

The Fritzsche's model uses the same modeling concept as the Wiedemann74 car-following model with the vehicle spacing ranging between the desired spacing (AD) and the risky spacing (AR). These two boundaries are determined as

$$AR = A_0 + T_r \times \frac{u_n}{3.6}\text{, and} \tag{23}$$

$$AD = A_0 + T_D \times \frac{u_{n-1}}{3.6}\,. \tag{24}$$

Where A_0 is the vehicle spacing at jam density, T_r is the risky time gap (usually 0.5 s), T_D is the desired time gap (with a recommended value of 1.8 s). The resulting steady-state car-following model can be written as

$$u_n(t+\Delta t) = \min\left\{\begin{array}{l} 3.6 \cdot \left(\dfrac{AD - A_0}{T_D}\right) \\ 3.6 \cdot \left(\dfrac{AR - A_0}{T_r}\right) \end{array}, u_f\right\} \tag{25}$$

The INTEGRATION car-following model, like the Gipps model, computes the vehicle speed as the minimum of the maximum vehicle speed based on vehicle dynamics and the desired speed based on the Van Aerde model formulation as

$$u_n(t+\Delta t) = \min\left\{\begin{array}{l} u_n(t) + 3.6 \cdot \dfrac{F_n(t) - R_n(t)}{m}\Delta t, \\ \dfrac{-c_1' + c_3 u_f + \tilde{s}_n(t) - \sqrt{\left[c_1' - c_3 u_f - \tilde{s}_n(t)\right]^2 - 4c_3\left[\tilde{s}_n(t)u_f - c_1' u_f - c_2\right]}}{2c_3} \end{array}\right\} \tag{26}$$

Steady-state Calibration

Rakha and Gao developed procedures for relating steady-state car-following model parameters to the four key macroscopic traffic stream parameters (u_f, u_c, q_c, and k_j), as summarized in Table 5. Using these calibration procedures the impact of inclement weather can be captured by adjusting the four traffic stream parameters using the WAFs that were presented earlier and then modifying the car-following parameters using the procedures of Table 5.

Table 5: Steady-State Model Calibration (Source: [20])

Car-following Model	Steady-State Calibration
Pitt Model	$c_3 = 3600\left(\frac{1}{q_c} - \frac{1}{k_j u_f}\right)$
Wiedemann 74	$E\left(BX\right) = 1000\sqrt{3.6}\sqrt{u_f}\left(\frac{1}{\alpha q_c} - \frac{1}{k_j u_f}\right)$ and $E\left(EX\right) = \frac{\frac{k_j u_f}{q_c} - 1}{\frac{k_j u_f}{\alpha q_c} - 1} \simeq \alpha$
Wiedemann 99	$CC0 = \frac{1000}{k_j} - \bar{L}$ $CC1 = 3600\left(\frac{1}{q_c} - \frac{1}{k_j u_f}\right)$
Gipps	b=b': $T = 2400\left(\frac{1}{q_c} - \frac{1}{k_j u_f}\right)$ b>b': Invalid behavior with a non-concave car-following relationship b<b': $b = \frac{1}{\left(\frac{1}{b'} + \frac{25920}{k_j u_c^2}\right)}$ and $T = 2.4\left(\frac{1000}{q_c} - \frac{1000}{k_j u_c} - \frac{u_c}{25.92b}\left(1 - \frac{b}{b'}\right)\right)$
Fritzsche	$A_0 = \frac{1000}{k_j}$; $T_D = 3600\left(\frac{1}{q_c} - \frac{1}{k_j u_f}\right)$; and $T_r = 3600\left(\frac{1}{q_c^{\max}} - \frac{1}{k_j u_f}\right)$
Van Aerde	$c_1 = \frac{u_f}{k_j u_c^2}\left(2u_c - u_f\right)$; $c_2 = \frac{u_f}{k_j u_c^2}\left(u_f - u_c\right)^2$; $c_3 = \left(\frac{1}{q_c} - \frac{u_f}{k_j u_c^2}\right)$

Table 6: Deceleration Model Calibration

Car-following	Model Deceleration Behavior
Pitt Model	Not possible given that b is fixed at 0.1.
Wiedemann 74	Assume $b_{min} = d_{max}$ in $$b_n(t) = \begin{cases} \frac{1}{2} \cdot \frac{\left[u_n(t) - u_{n-1}(t)\right]^2}{ABX - \left[\Delta x_n(t) - L_{n-1}\right]} + b_{n-1}(t) + b_{\min} \cdot \frac{ABX - \left[\Delta x_n(t) - L_{n-1}\right]}{BX} & s_n(t) \le ABX \\ \frac{1}{2} \cdot \frac{\left[u_n(t) - u_{n-1}(t)\right]^2}{ABX - \left[\Delta x_n(t) - L_{n-1}\right]} + b_{n-1}(t) & s_n(t) > ABX \end{cases}$$
Wiedemann 99	Not possible.
Gipps	b' $=d_{max}$ and $b = \frac{1}{\left(\frac{1}{b'} + \frac{25920}{k_j u_c^2}\right)}$
Fritzsche	$b_{min} = d_{max}$ and $u_n(t + \Delta t) = \frac{s_n(t) + \frac{\left(u_{n-1}(t) - u_n(t)\right)^2}{\left\|b_{\min}\right\| + b_{n-1}(t)} - A_0}{T_r}$
Van Aerde	b=d_{max} and $c_1' = \frac{u_f}{k_j u_c^2}\left(2u_c - u_f\right) + \max\left(\frac{u_n^2(t) - u_{n-1}^2(t)}{2b}, 0\right)$.

Deceleration Calibration

In addition to adjusting the steady-state car-following behavior, vehicle deceleration and acceleration parameters can be adjusted to reflect wet roadway conditions using the parameter values that were presented earlier in Table 2 and Table 3. Specifically, in the case of deceleration model calibration, a summary of key parameters and proposed values are presented in Table 6. The CORSIM software does not allow for the calibration of vehicle deceleration levels nor does the VISSIM Wiedemann99 model. In the case of the Wiedemann74 model the impact of wet roadway conditions can be captured by equating the maximum deceleration rate (b_{min}) with the maximum possible deceleration rate computed in Equation (3) for the specified rain intensity level. Similarly, in the case of the Gipps, Fritzsche, and Van Aerde model the $b\,'$, b_{min}, and b parameters can be set equal to the maximum deceleration rate for a specific rain precipitation intensity computed using Equation (3), respectively.

Acceleration Calibration

The calibration of vehicle acceleration behavior under inclement weather is briefly described in this section.

In the case of the CORSIM, Paramics, and VISSIM software the modeler can provide an speed-acceleration relationship. The relationship can be derived using the vehicle dynamics procedures described earlier.

In the case of the AIMSUN2 software, the desired vehicle acceleration rate can be computed using Equation (4) as

$$a_{max} = f_p \frac{F - R}{m} = f_p \left[\min\left(\frac{K_T \beta}{u}, \frac{m_{ta}}{m} g\mu \right) - \left(K_a u^2 + K_{r1} u + K_{r2} + gi \right) \right]. \quad (27)$$

Given that the maximum acceleration occurs as the vehicle speed approaches zero, the maximum sustainable force between the roadway surface and the vehicle tires becomes the governing factor (F_{max}). Consequently, the desired maximum acceleration rate can be computed as

$$a_{max} = f_p g \left(\frac{m_{ta}}{m} \mu - \frac{C_r c_3}{1000} \right) - f_p gi = a^0_{max} - f_p gi \,. \quad (28)$$

Here g is the gravitational acceleration of 9.8066 m/s^2 and $a^0{}_{max}$ is the maximum acceleration for a level surface (grade of 0%). The advantage of Equation (28) is that it relates the maximum desired acceleration to vehicle, roadway, and driver characteristics. Driver characteristics are accounted for using the f_p parameter, which is the proportion of the maximum acceleration that the driver is willing to exert. All other terms in Equation (28) are related to the vehicle and roadway characteristics.

In the case of heavy-duty trucks (weight-to-power ratio > 30 kg/kW) the maximum acceleration is constrained by the engine tractive force as opposed to the maximum sustainable force between the vehicle tires and roadway surface. Experimentation with various truck data demonstrated that the best fit is obtained for a speed of 2 km/h, as will be demonstrated later in the paper. Consequently, the maximum acceleration is computed as

$$a_{max} = f_p \left[\frac{K_T}{u_0} \left(1.5 - \frac{1}{u_0} \right) - 4K_a - 2K_{r1} - K_{r2} - gi \right] = a_{max}^0 - f_p gi \,. \quad (29)$$

In the case of the INTEGRATION software the calibration of vehicle acceleration behavior is achieved by changing the coefficient of road adhesion and the rolling coefficient given that the model uses the vehicle dynamics approach that was described earlier in the paper.

EXAMPLE MODEL APPLICATION

For illustration purposes the proposed calibration approach is applied to the INTEGRATION software for the modeling of a section of the I-81 Interstate Highway. The section of I-81 extends from Christiansburg, VA to Roanoke, VA, which corresponds to mileposts 118 to 143. This section is basically a two-lane per direction highway with some three-lane segments to accommodate the slower moving trucks [21]. This section initially describes the network construction and calibration effort, the various scenarios that were simulated, and the study results.

Model Construction and Calibration

The simulation network construction involved building a network from AutoCAD designs. This design was used to define the horizontal and vertical profile with a high degree of accuracy. Base lane characteristics in terms of capacity, free-flow speed, speed-at-capacity, and jam density were derived using the Highway Capacity Manual (HCM) procedures for a basic freeway section. The impact on lane changing and heavy vehicles on the base roadway parameters was captured using the simulation software. These impacts have been validated in a number of studies [38, 39].

Trucks were modelled based on an earlier research effort that characterized the trucks along the study section of I-81 [22, 23]. Two types of trucks were modeled, namely a truck with a 20,411 kg mass and engine power of 336 kW (67%) and another with a mass of 31,751 kg and an engine power of 261 kW (33%).

Light duty vehicles were modelled as light-duty vehicle 3 (LDV3), which is a vehicle of model year 1995 or later, an engine size less than 3.2 L, and an average mileage of less than 83,653 km. The use of different vehicle types would affect the absolute fuel consumption and emission estimates of the various scenarios, but should not affect the relative values given that all scenarios were modeled using the same vehicle composition.

The 2004 existing peak hour traffic volumes and the 2035 design hour traffic volumes were provided in the I-81 Corridor Improvement Study Technical Report. Using the two sets of volume counts link specific growth rates were computed. These growth rates varied between 0.0% and 3.6% in the case of light duty vehicles and 2.3% and 3.0% in the case of the heavy duty trucks depending on the link under consideration. Using the average annual growth rates, the traffic volumes for 2020 and 2035 were computed.

Given the projected traffic volumes, the next step in the analysis was to compute the O-D matrix for use as input to the simulation software. The calibration of O-D demands to field observed link flows is a problem that has been the focus of extensive research. The most renowned of the approaches is the maximum likelihood approach that was first formulated by Van Zuylen and Willumsen [32] and Willumsen [33] and by Van Aerde *et al*. . The traffic demands for the individual model years were estimated using a maximum likelihood synthetic O-D estimation software entitled QUEENSOD [34-37]. The QUEENSOD software estimates the maximum likelihood O-D table that replicates the observed link flows (projected link flows here). The numerical solution begins by building a minimum path tree and performing an all-or-nothing traffic assignment of the seed matrix. A relative or absolute link flow error is computed depending on user input. Using the link-flow errors, O-D adjustment factors are computed and utilized to modify the seed O-D matrix. The adjustment of the O-D matrix continues until one of two criteria are met, namely the change in O-D error reaches a user-specified minimum or the number of iterations criterion is met.

The analysis considered four scenarios that involved different strategies for managing truck and general purpose lanes, including the "Do-Nothing" scenario. These strategies included modifications to three sub-sections along I-81. The scenarios are as follows:

- **Scenario 1 (S1). Do-nothing:** Represents the base case do-nothing scenario.
- **Scenario 2 (S2).** This scenario involves the addition of a single lane along section 2 (milepost 125 to 120.7). In addition, the leftmost lane is restricted to light duty vehicles for the three sub-sections (from milepost 128.1 to 119.6).
- **Scenario 3 (S3).** This scenario involved the addition of a single lane across all three sub-sections (i.e. from milepost 128.1 to 119.6). The two leftmost lanes were restricted to light duty vehicles for sub-sections 1 and 3 while the leftmost lane was restricted to light duty vehicles along the 3-lane sub-section from milepost 125.0 to 120.7 (sub-section 2).
- **Scenario 4 (S4).** This scenario was identical to scenario 3 with the addition of a forth lane along sub-section 2 (from milepost 125.0 to 120.7). The two leftmost lanes were restricted to light duty vehicles for the three sub-sections.

Having generated the O-D tables for the model years of 2004 through 2035 at 5-year increments, three individual scenarios were simulated using the INTEGRATION microscopic traffic simulation software. Specifically, each scenario was simulated 20 times with a different random number seed for each model year to introduce randomness into the simulation results. Thus, a total of 560 simulation runs were conducted (20 random number seeds x 4 scenarios x 7 model years).

Inclement Weather Impacts

The various scenarios were simulated considering different levels of rain and snow precipitation. The impact of inclement weather was captured by modifying three basic roadway parameters, namely: free-flow speed, speed-at-capacity, and capacity using the WAFs that were presented earlier in Table 1. In addition, the roadway rolling coefficient

and coefficient of roadway adhesion were adjusted to reflect different roadway surface conditions using the values that were presented earlier in Table 3.

The average speed was analyzed for each of the four scenarios considering different rain precipitation levels for the entire traffic stream, light-duty vehicles only, and heavy-duty trucks, as illustrated in Figure 2. The results demonstrate that the average speed for cars is approximately equal to the free-flow speed across the various scenarios under ideal weather conditions (ranges between 64.8 and 67.0 mi/h). Alternatively, the heavy-duty trucks travel at much lower speeds, ranging from 46.5 to 48.0 mi/h, as a result of the significant grade sections along the study corridor. Figure 2 demonstrates that the introduction of rain results in a 5% reduction in the light-duty vehicle speeds and a 3% reduction in the heavy-duty vehicle speeds. An increase in the rain intensity further reduces light-duty vehicle and heavy-duty truck speeds resulting in a maximum reduction of 8.5% and 4.5% at the maximum rain intensity of 1.5 cm/h, respectively. The results also demonstrate that the impact of rain on the traffic stream speed is more significant than the differences in traffic stream speed across the various scenarios and thus is a factor that should be considered in the analysis of traffic operational projects.

The traffic scenarios were also compared using the 2020 demand, as illustrated in Figure 3. The growth in traffic demand results in a decrease in the average light-duty vehicle speed from the range of 64.8 to 67.0 mi/h to 61.0 to 64.3 mi/h (a reduction of approximately 6%). This reduction in the average speed is equivalent to the reduction produced by a 0.3 cm/h rain precipitation (i.e. the minimum rain precipitation produces reductions in traffic stream speed equivalent to a 16-year traffic growth). Heavy-duty truck speeds are reduced from the 46.5 to 48.0 mi/h range to 43.1 to 45.0 mi/h for the 2004 and 2020 demand levels, respectively. The impact of rain intensity on the average traffic stream speed appears to increase as the level of congestion increases, as demonstrated by comparing Figure 2 to Figure 3. Specifically, reductions in average speeds in the range of 9.7% and 5.8% are observed for the 2020 demand for the maximum rain intensity of 1.5 cm/h for light-duty and heavy-duty vehicles, respectively.

Similarly the results for the 2035 demand resulted in an additional reduction in light duty vehicle speeds in the range of 12% to 16% and a reduction in heavy-duty truck speeds in the range of 6% to 10%. Consequently, it can be concluded that the impact of rain precipitation on traffic stream speed increases as the level of congestion within the network increases.

The results also demonstrate that the rain intensity has no impact on the relative merit of the various scenarios (i.e. the ranking of the scenario results are consistent across the various rain intensity levels). This finding is important given that it demonstrates that a recommendation on the optimal scenario is not impacted by the weather conditions that are considered in the analysis.

In the case of snow precipitation, the average light-duty vehicle speed and heavy-truck speed is reduced by approximately 55% by the precipitation on snow on the roadway surface as a result of a reduction in the roadway rolling and adhesion coefficients, as demonstrated in Figure 4. An increase in the snow precipitation intensity does not appear to produce any further reductions in the average traffic stream speed, as illustrated in Figure 4.

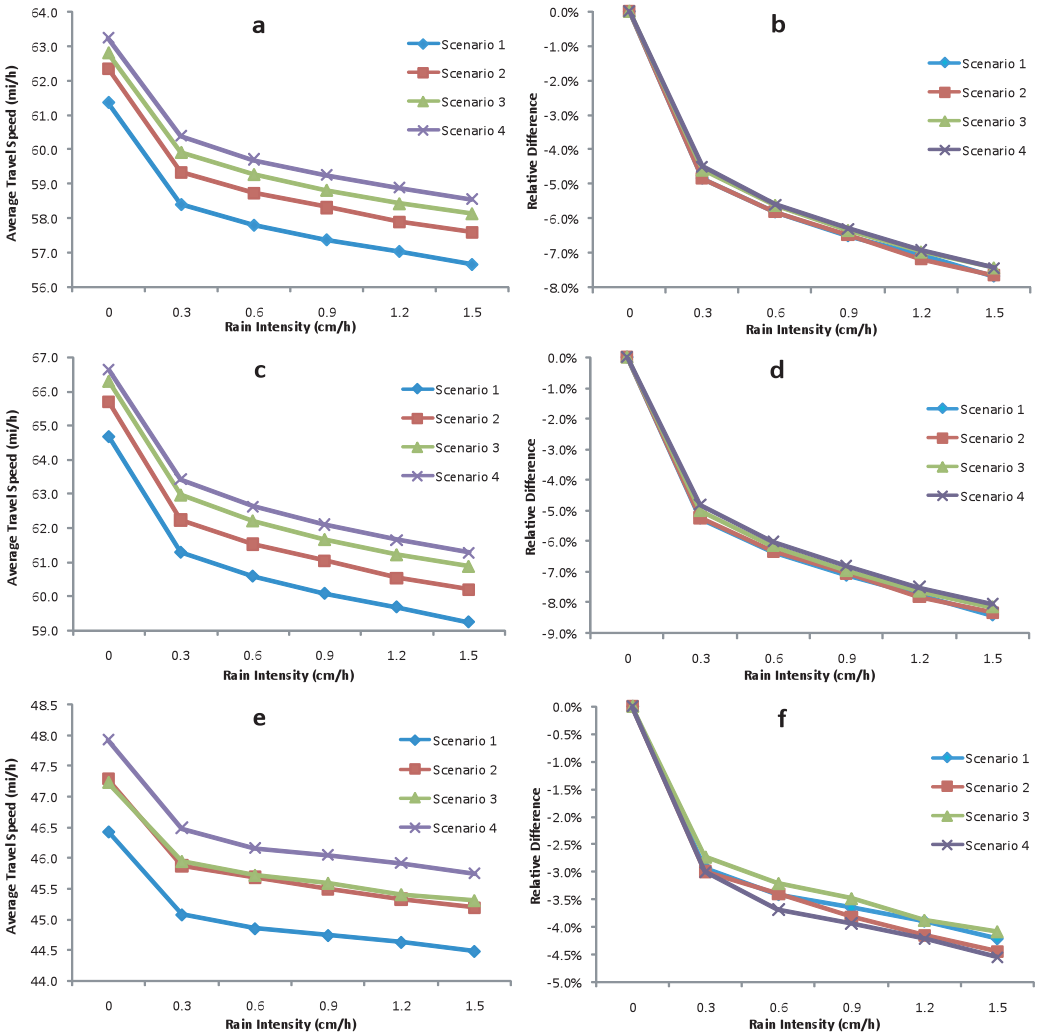

Figure 2: Average Travel Speed Variation as a Function of Rain Intensity for 2004 Traffic Demand (a, b) All vehicles, (c, d) Cars, and (e, f) Trucks

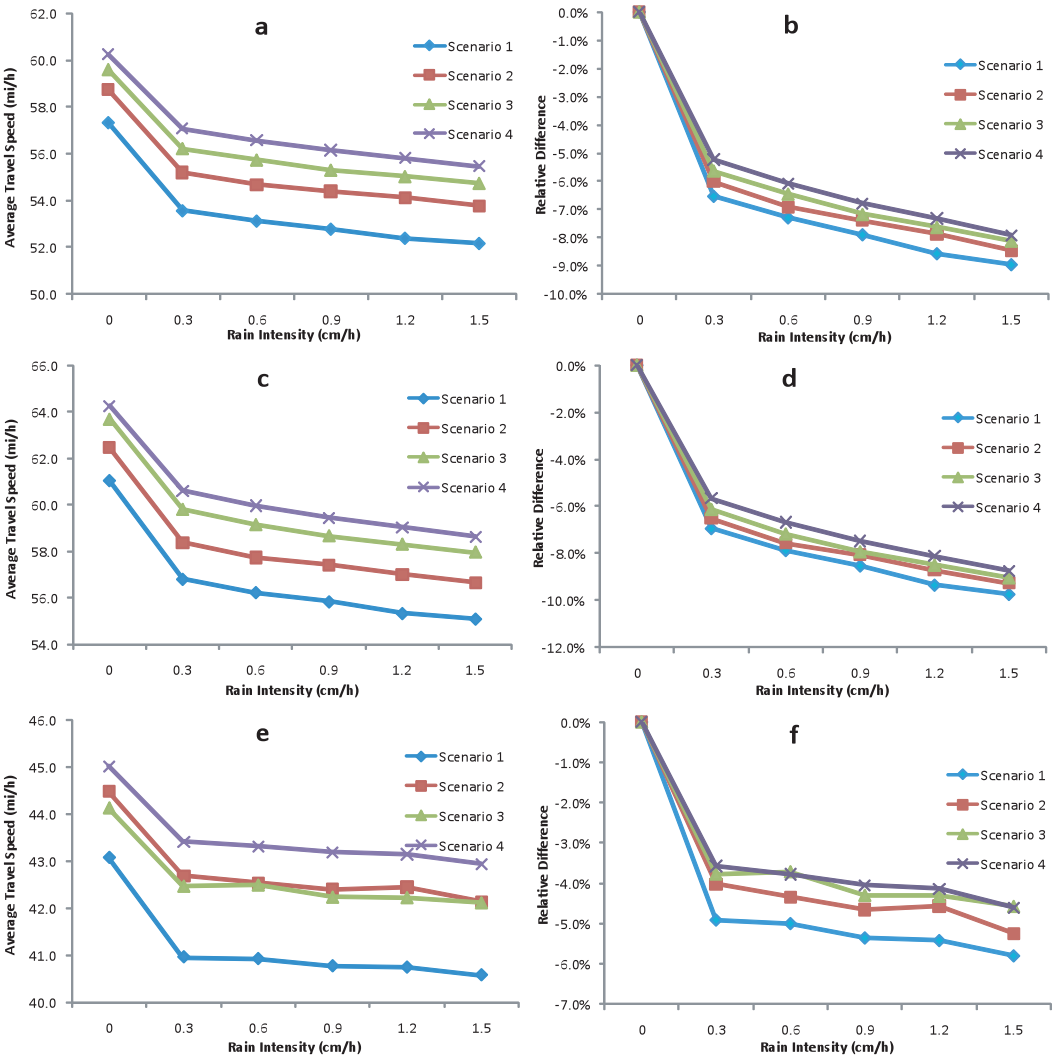

Figure 3: Average Travel Speed Variation as a Function of Rain Intensity for 2020 Traffic Demand (a, b) All vehicles, (c, d) Cars, and (e, f) Trucks

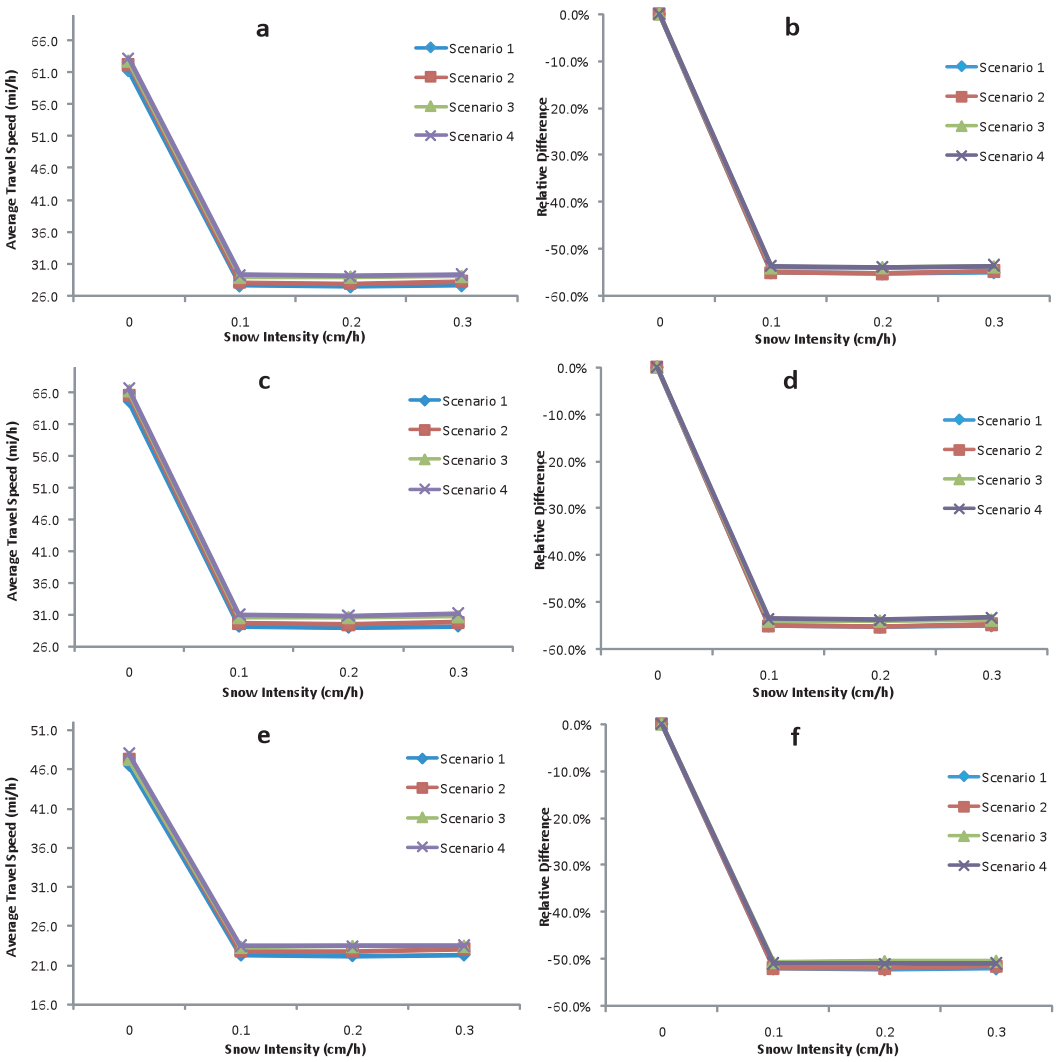

Figure 4: Average Travel Speed Variation as a Function of Snow Intensity for 2035 Traffic Demand (a, b) All vehicles, (c, d) Cars, and (e, f) Trucks

CONCLUSIONS

The research identified the steady-state car-following model parameters that require calibration to reflect inclement weather and roadway conditions, developed procedures for calibrating non-steady state car-following models to capture inclement weather impacts, and applied the procedures to a sample network. The results demonstrate that the introduction of rain precipitation results in somewhere in the range of a 5% reduction in the light-duty vehicle speeds and a 3% reduction in heavy-duty vehicle speeds. An increase in the rain intensity further reduces light-duty vehicle and heavy-duty truck speeds resulting in a maximum reduction of 9.5% and 5.5% at the maximum rain intensity of 1.5 cm/h, respectively. The results also demonstrate that the impact of rain on traffic stream speed increases with the level of congestion and is more significant than speed differences attributed to various traffic operational improvements and thus should be accounted for in the analysis of alternatives. In the case of snow precipitation, the speed reductions are much more significant (in the range of 55%). Furthermore, the speed reductions are minimally impacted by the snow precipitation intensity. The study further demonstrates that precipitation intensity has no impact on the relative merit of the various scenarios (i.e. the ranking of the scenario results are consistent across the various rain intensity levels). This finding is important given that it demonstrates that a recommendation on the optimal scenario is not impacted by the weather conditions that are considered in the analysis.

ACKNOWLEDGEMENTS

The authors acknowledge the valuable input from Dr. William Perez of Cambridge Systematics, Inc. and Roemer Alfelor and David Yang of the Federal Highway Administration. Finally, the authors acknowledge the financial support provided by the FHWA in conducting this research effort.

REFERENCES

1. TRB, *Highway Capacity Manual 2000*. 2000: Transportation Research Board.
2. Rakha, H., P. Pasumarthy, and S. Adjerid. *The INTEGRATION framework for modeling longitudinal vehicle motion*. in *TRANSTEC*. 2004. Athens, Greece.
3. Ozaki, H., *Reaction and Anticipation in the Car-following Behavior*, in *12th International Symposium on Transportation and Traffic Theory*. 1993, Elsevier. p. 349-366.
4. Rakha, H.A. *Validation of Van Aerde's simplified steady-state car-following and traffic stream model*. in *85th Transportation Research Board Annual Meeting*. 2006. Washington D.C.: Transportation Research Board.
5. Gazis, D., R. Herman, and R. Rothery, *Nonlinear follow-the-lead models of traffic flow.* Operations Research, 1961. 9(4): p. 545-567.
6. Dowling, R., et al., *Guideline for Calibration of Micro-simulation Models: Framework and Applications*. Transportation Research Record, 2004. 1876: p. 1-9.
7. Rakha, H., et al. *Inclement Weather Impacts on Freeway Traffic Stream Behavior*. in *Transportation Research Board 87th Annual Meeting*. 2008. Washington D.C.
8. MINITAB, *User's guide 2: Data analysis and quality tools*.
9. Mannering, F.L. and W.P. Kilareski, *Principles of Highway Engineering and Traffic Analysis*. Second ed. 1998: John Wiley & Sons.

10. Rakha, H., et al., *Vehicle dynamics model for predicting maximum truck acceleration levels*. Journal of Transportation Engineering, 2001. 127(5): p. 418-425.
11. Rakha, H. and I. Lucic, *Variable power vehicle dynamics model for estimating maximum truck acceleration levels*. Journal of Transportation Engineering, 2002. 128(5): p. 412-419.
12. Rakha, H., M. Snare, and F. Dion, *Vehicle dynamics model for estimating maximum light-duty vehicle acceleration levels*. Transportation Research Record, 2004. n 1883: p. 40-49.
13. Halati, A., H. Lieu, and S. Walker, *CORSIM- Corridor Traffic Simulation Model* in *76th Transportation Research Board Meeting*. 1997: Washington DC.
14. Gipps, P.G., *A behavioral car-following model for computer simulation*. Transportation Research, 1981. 15B: p. 105-111.
15. Rakha, H., C.C. Pecker, and H.B.B. Cybis. *Calibration procedure for the Gipps' car-following model*. in *86th Transportation Research Board Annual Meeting*. 2007. Washington, DC: Transportation Research Board.
16. Wilson, R.E., *An analysis of Gipps' car-following model of highway traffic*. IMA Journal of Applied Mathematics, 2001. 66: p. 509-537.
17. Fritzsche, H.T., *A model for traffic simulation*. Traffic Engineering and Control, 1994. 5: p. 317-321.
18. Van Aerde, M., *Single regime speed-flow-density relationship for congested and uncongested highways*. Presented at the 74th TRB Annual Conference, Washington DC, Paper No. 950802., 1995.
19. Van Aerde, M. and H. Rakha. *Multivariate calibration of single regime speed-flow-density relationships*. in *Proceedings of the 6th 1995 Vehicle Navigation and Information Systems Conference*. 1995. Seattle, WA, USA: Vehicle Navigation and Information Systems Conference (VNIS) 1995. IEEE, Piscataway, NJ, USA,95CH35776..
20. Rakha, H. and Y. Gao. *Calibration of Steady-state Car-following Models using Macroscopic Loop Detector Data*. in *Symposium on The Fundamental Diagram: 75 Years*. 2008. Woods Hole, MA.
21. Rakha, H., et al., *Evaluating Alternative Lane Management Strategies along I-81*. Transportation Research Board 84 th Annual Meeting, Washington D.C., 2005.
22. Dion, F., H. Rakha, and Y. Zhang, *Evaluation of Potential Transit Signal Priority Benefits along a Fixed-Time Signalized Arterial*. Journal of transportation engineering, 2004. 130(3): p. 10.